International Journal of Computing and Digital Systems
ISSN (2210-142X)
Int. J. Com. Dig. Sys. 14, No.1 (Sep-2023)

http://dx.doi.org/10.12785/ijcds/140154

Impact Assessment of Redox Flow Battery Coordinated Diverse Link on Frequency Regulation in Multi-Area Multi-Source Power System with Decentralized Optimal Control

Archana Singh[1] **and Sathans Suhag**[2]

[1]*School of Renewable Energy and Efficiency, National Institute of Technology, Kurukshetra, Haryana, India*
[2]*Department of Electrical Engineering, National Institute of Technology, Kurukshetra, Haryana, India*

Received 01 Jul. 2022, Revised 22 May 2023, Accepted 31 Jul. 2023, Published 01 Sep. 2023

Abstract: The study explores the potential of redox flow battery in regulating frequency in large interconnected power system having coupled diverse links - AC and HVDC Links, and thyristor controlled phase shifter -, and compares its performance against other energy storage devices, employing linear quadratic regulator based decentralised optimal control. Also, the impact of the diverse links on frequency regulation is examined in coordination with redox flow battery. The system comprises four equal areas, containing reheat thermal turbine and electrical vehicle aggregator as generating sources in each area, step and random changes (wind and photovoltaic power uncertainties) in load as the disturbances. The suggested controller, coordinated with redox flow battery and diverse links, settles system frequency and tie-line power excursions in quickest possible duration as against conventional PI and PID control. The proposition is also tested effective against time delay non-linearity in system. Simulations are executed on MATLAB platform with results analysed and illustrated in a lucid manner.

Keywords: Interconnected power system, Frequency regulation, Linear quadratic regulator, Optimal controller, Redox flow battery.

1. INTRODUCTION

Frequency regulation has got huge significance for large IPS and more so with the expansion and integration of power scenario, especially when power system is seeing big changes due to installation of ESDs, FACTS, distributed, and renewable energy sources. Any mismatch in active power and load leads to frequency and tie-line power excursions adversely affecting stability in power system. ESDs such as RFB, SMES, UCs are active power sources, quick and most effective along with generating sources and help to minimise frequency excursion, regulate faster and compensate sudden load variation in one power area [1]. Automatic generation control with FACTS devices mitigates tie line power oscillations and improves system performance effectively [2]. HVDC interconnection also supports inertia in low inertia power system, minimises frequency regulation along with numerous advantages in terms of power transfer capability, flexibility, being economic over long transmission line [3]. Besides, HVDC also helps maintain frequency by way of dynamical adjustments of power output [4]. Coordinated placement of FACTS devices along with ESDs improves system performance more effectively. Frequency regulation of hydropower system, utilizing synergy of RFB and TCPS, is presented in [5], while authors in [6] present the findings on damping of frequency oscillations for a system comprising wind turbine, TCPS, and SMES. Power system performance with various FACT devices and SMES is compared and analysed in [7]. In [8], performance of non-linear power system integrated with wind turbine generator (WTG) improves with coordinated action of TCPS and SMES.

Literature presented in [9] [10] [11] [12] demonstrates RFB as the most economic ESD, requiring less maintenance and having longer life, therefore best suited in power system for regulating frequency and other applications.

Importance of RFB in renewable energy sources is described in [12], while LFC performance improvement with RFB and interline power flow controller (IPFC) is presented [13]. Extensive benefits of RFBs include independently tuneable power rating, quick response nature, long life, load-levelling and no self-discharge etc. compared to similar ESDs like SMES, and UC and hence RFBs find more appropriate applications in grid connected power system [9]. Comparative study of these similar performing ESDs in power connected grid is given in Table-I. Flexible operations, ease of recycling, large capacity, high efficiency

E-mail address: archu_singh20@rediffmail.com, sathans@nitkkr.ac.in

are some more features of RFB over other ESDs to get more attention in current high renewable energy penetrated power scenario. RFBs have longer life span with unlimited number of charging/discharging cycles without degradation of battery and electrolytes of RFBs are semi-permanent type. Recently many researchers have presented different controller design approaches for multi area LFCs with various advanced methodologies considering impact of FACTS, HVDC and ESDs Tungadio et al. [14] presented deep review work on LFC considering renewable energy sources and energy storages as a part of generating sources with traditional and modern/predictive controllers. Irfan Ahmed Khan et al. [15] presented review on LFC control study on future LFC trend for large-area hybrid power systems including various ESDs and FACTS devices coupled with HVDC tie lines.

Pandey et al. [16] extensively reviewed LFC challenges for IPS incorporated with ESDs, FACT devices and renewable energy sources. Fathy et al. [17] details fractional-order PID LFC for multi area network with renewable energy penetration. Ko et al. [18] described Lyapunov theory with linear matrix inequalities to deal with time delay in LFC of an IPS with EV aggregator. Hybrid bacterial foraging enhanced particle swarm optimization tuned controller is presented for IPS in [19]. These studied controllers are highly computational and take substantially large time in computing controller parameters, while LQR is one of the most popular and robust controllers, which is found significant in large IPS with the limitation that the transfer of information from one area to other may be distorted and delayed. Considering large IPS, distributed controllers, which need to be designed for individual areas and placed in same areas, are suggested in recent studies [20], [21], [22], [23], [24]. Authors in [20] presented Kalman filter based controller, while in [21] is presented the distributed linear functional observer controller which is having limitation of considering few outputs of other areas to design controller of other areas to fulfil observability condition, meaning thereby that it's not completely distributed controller. Fully decentralised observer controller with online estimation of disturbances is described in [22]. Authors in [23] presented quasi-decentralised observer based optimal controller whereas, while in [24] is detailed the distributed LQR controller which utilises top-down methodologies to approximate centralised LQR controller. Evolutionary optimized PID controllers take long computational time, while most of the LQR based controllers utilise all/many states of the other areas in designing the decentralised controllers, meaning thereby that they are not fully de-centralised controllers.

A. Related Work

Frequency and power excursions are two of the major stability issues which are increasing owing to integration of renewable and multi sources into power network. ESDs coordinated with diverse links counter the instability and reduce oscillations of system frequency and tie line power. Improved performance has been reported in [25] for two area power system with integration of RFB in power area and TCPS in tie line during sudden solar irradiance change and fast changing demand load. Fast responding behaviour of RFB and super Capacitor (SC) are able to counter large and sudden variation of load required in current era of power scenario [26]. LFC performance improves with placement of RFB and UC in power areas [27]. Performance of multi-source multi-area power network is enhanced through placement of SMES coordinated TCSC (Thyristor controlled series compensator) [28]. In [29], authors compared and contrasted the power system performance with and without SMES and HVDC link, and concluded that system dynamics improved by integration of SMES and HVDC link. Mausri Bhuyan [30] presented improved performance of two power areas interconnected via AC/HVDC link integrated with SMES and BESS in each area. Optimal controller designed for hydro-hydro power system integrated with RFB is effective in improving frequency response in deregulated scenario as claimed in [31]. Comparative analysis of recent related works, including the instant study, is presented in TABLE II.

With this background, the instant study designs and implements the distributed LQR based optimal controller for a large IPS integrated with different ESDs and diverse links which is relatively easier in design, less complicated and requires least transfer of information from one area to other area to design controllers as compared to centralised optimal controller. There are five sections in total which this study is organized into, with section 1 introducing and setting the background for the instant study citing relevant literature. System modelling using transfer function approach is the focus of section 2, while section 3 presents state space modelling and the controller design. Simulation findings are illustrated and analysed in section 4 and concluded in section 5.

2. SYSTEM DESCRIPTION

Four reheat thermal power areas interconnected with AC/HVDC link and TCPS, and each area having coupled EV, and ESDs, constitute the system which is exposed to step load change and renewable energy like disturbances. Fig. 1(a and b) portray the any one (i^{th}) area of the system and interconnection of four areas, respectively. Each component of the system is briefly described as follows:

A. Reheated Thermal Turbine

Reheated thermal turbine comprises generator, turbine, and reheater unit, transfer function model and dynamics of each of these is expressed as below.

$$\Delta X_{gi} = \frac{K_{gi}}{sT_{gi}+1}\Delta P_{cgi}. \tag{1}$$

$$\Delta P_{ri} = \frac{K_{ti}}{sT_{ti}+1}\Delta X_{gi}. \tag{2}$$

$$\Delta P_{gi} = \frac{sK_{ri}+1}{sT_{ri}+1}\Delta P_{ri}. \tag{3}$$

TABLE I. Comparative study of RFB, SMES, UC [9]-[12]

	RFB	SMES	UC
Advantages	1) High energy storage capacity 2) High efficiency (upto 85 %) 3) Moderate power density (75-150 w/kg) 4) Very quick response 5) Least combustible 6) No self-discharge 7) Highly flexible 8) Highly versatile 9) Economical	1) Fast response 2) High efficiency (upto 90 %) 3) High reliability 4) 10 - 15 % self-discharge 5) High energy density	1) High power density (2000-5000 W/Kg) 2) Long life cycle (105 to 107) 3) High efficiency (upto 95 %)
Disdvantages	1) Low energy density (35-60 Wh/kg) 2) Complex construction	1) High cost due to cryogenic system 2) Very low operating temperature(-270°C) required to generate magnetic fields 3) Requires high magnetic fields	1) Life cycle depends on voltage imbalance 2) Safety problem 3) Environment implication 4) Low energy density (3-5 Wh/kg)
Energy carrier	Electrolytes	Electromagnetic	Electrostatic
Applications	Load shifting, Frequency regulation, Renewable energy sources	Short time applications: Power quality, Pulse source for FACTS and UPS	Frequency regulation and voltage regulation

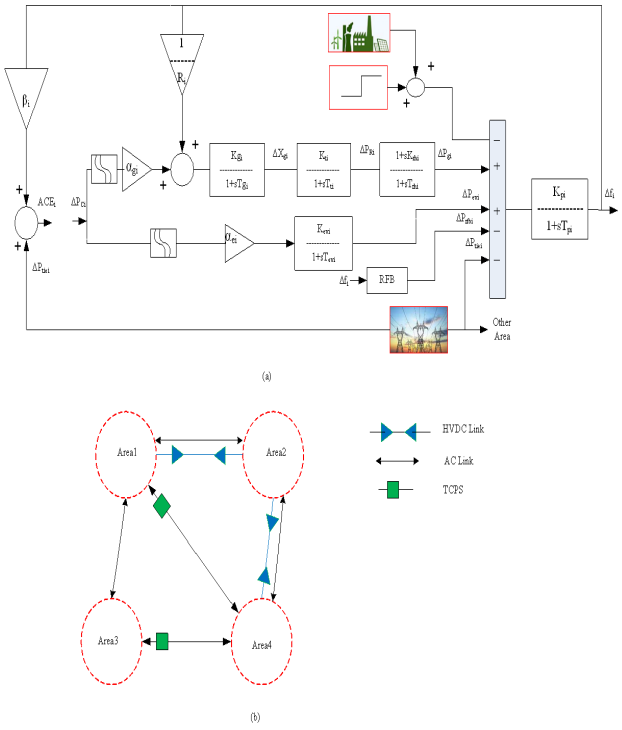

Figure 1. System under study: a) i^{th} Area diagram b) Interconnection of 4 area power system

Where K_{gi}, T_{gi}, K_{ri}, T_{ri}, and K_{ti}, T_{ti} notify gain and time constant pairs associated with governor, reheater units, and turbine, respectively, while ΔX_{gi}, ΔP_{cgi}, ΔP_{ri} and ΔX_{gi}, ΔP_{gi} andΔP_{ri} are the change in output and input of governor, turbine, and reheater units, respectively.

B. Electrical Vehicles

EVs are connected to grid via bidirectional power electronics devices and they react faster than any other conventional generator for load perturbations. Large no. of EVs pump energy to grid when they are parked at station and constitute behave as power source and participate in LFC to support generating units. Power dynamics of EVs are modelled as first order transfer function and written as [17][21].

$$\Delta P_{evi} = \frac{K_{evi}}{sT_{evi}+1}\Delta P_{cei}. \tag{4}$$

Where, K_{evi} and T_{evi} denote gain and time constant, while ΔP_{evi} and ΔP_{cei}, respectively, represent output and input of EV at ith area.

C. Redox Flow Battery

Vanadium RFBs serve as very prominent ESDs which comprise two vanadium electrolytes which exchange hydrogen ions through a membrane based on the electrochemical reaction theory. Sulphuric acid doped with vanadium ions constitutes the electrolytic solution of RFBs to support the chemical reactions. Vanadium ions $V^{(4+)}/V^{(5+)}$ are utilised as positive electrode, while $V^{(2+)}/V^{(3+)}$ as negative electrode

TABLE II. Comparative analysis with recent work

Reference No.	ESDs used	links coordinated with AC tie line	No. of power Areas	Power generation Sources	Controller used	Special Features Computational Complexity	Non-Linearity considered	Uncertainties included
[1]	UC, SMES, RFB	-	3	Reheat thermal turbine	Fuzzy PID	high	-	-
[7]	SMES	TCPS	2	SG, DFIG	Tie line bias control	-	-	-
[25]	RFB	TCPS	2	Diesel, Hydro and Thermal, Solar Park	Type 2 LFC	high	GRC	Step loading
[26]	SC and RFB	-	2	Geo thermal power plant, solar thermal power system	1+TDF	high	Solar and wind	Random loading
[27]	UC and RFB	-	2	Hydro power plant	Fuzzy PID	high	-	Unit step and random loading
[28]	SMES	TCSC	2	Thermal, hydro, Gas	PID	high	-	Random loading
[29]	SMES	HVDC	3	HDGT (heavy duty gas), Solar Chimney, BDPG	TDF	high	-	Step loading
[30]	BESS, SMES	HVDC	2	(Bio Diesel powered generator) CSGT (combined solar gas turbine)	PI-TID	high	-	Random loading
[31]	RFB	-	2	Hydro-Hydro	Optimal	Easy to compute	GRC	Random loading
Instant Study	RFB SMES UC FESS, and conventional BESS	HVDC, TCPS	4	Thermal, EV	Distributed Optimal controller	Easy to compute	Solar, Wind	Time delays, Unit step loading

and during charging, $V^{(3+)}$ is converted into $V^{(2+)}$ and $V^{(5+)}$ into $V^{(4+)}$ and vice versa during discharging.

RFBs with two isolation chambers avoid self-discharging problem and the charge/discharge cycles are regulated through oxidation and reduction reactions of the electrolytic solution. Sensors, pumps, secondary containment vessel, power and flow management are the important components of RFB and the volume of electrolyte solution decides its operating range. Figures 2 (a and b), respectively, illustrate the working schematic diagram and small signal transfer function representation.

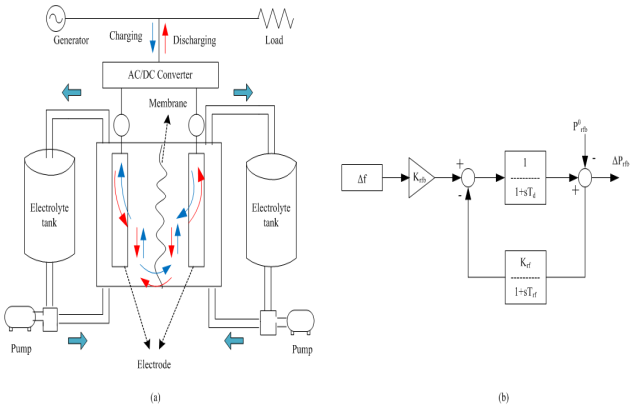

Figure 2. RFB: a) Working principle diagram b) Transfer function model

Dynamics of RFB are expressed in equation (5) as referred in [32][33].

$$\Delta P_{rfbi} = \left(K_{rfbi}\Delta f_i - \frac{K_{rfi}}{sT_{rfi}+1}(\Delta P_{rfbi} - \Delta P^0_{rfbi})\right)\frac{1}{sT_{di}+1}. \quad (5)$$

Where, $T_{di} = 0$, Set value $P^0_{rfbi} = 0, K_{rfbi}$ is RFB gain constant, K_{rfi} and T_{rfi} notify reset gain and time constant, while ΔP_{rfbi}, in the usual sense of the symbol, is the output power of RFB.

D. Modelling of Interconnections

HVDC Link- Small signal dynamics of power exchange of HVDC link between two areas at ith area is given as

$$\Delta P_{dci} = \frac{K_{dcij}}{sT_{dcij}+1}(\Delta f_i(s) - \Delta f_j(s)). \quad (6)$$

And power exchange of HVDC link among N interconnected areas at ith area is given as

$$\Delta P_{dci} = \frac{K_{dcij}}{sT_{dcij}+1}\Sigma^N_{j=1,j\neq i}K_{dcij}(\Delta f_i(s) - \Delta f_j(s)). \quad (7)$$

Where, Δf_i is the frequency deviation of ith area, $K_{dcij} = 1$ signifies that the interconnection exists, while $K_{dcij} = 0$ indicates that HVDC is not connected between areas [21] [23].

AC Link with TCPS- Linearized incremental power model of AC link with TCPS, both connected in series and placed near ith area, is given as below [5], [8].

$$\Delta P_{acij} = \frac{2\pi T_{ij}}{s}(\Delta f_i(s) - \Delta f_j(s)) + T_{ij}\Delta\phi_{tcps}. \quad (8)$$

Where, $\Delta\phi_{tcps}$ is phase angle of TCPS which is varying with change in frequency and it can be used as control signal for tie line and related as

$$\Delta\phi_{tcps} = \frac{2\pi K_{TCPS}}{sT_{tcps}+1}\Delta f_i. \quad (9)$$

T_{tcps} and K_{tcps} represent time and gain constants, respectively, of TCPS, while T_{12} is synchronising coefficient for AC link. Total tie line power deviations at ith area from other areas are modelled as

$$\Delta P_{tiei} = \Delta P_{acij} + P_{dci} \quad (10)$$

3. LQR BASED DISTRIBUTED OPTIMAL CONTROLLER

To design distributed controller, tie line power of each area has been considered as disturbance vector along with load perturbation in state space modelling of system, and state feedback control gain is first computed for each area.

A. State Space Modelling of System

For the purpose, state vector considered for ith area without RFB is $x_i(t) = \{\Delta f_i, \Delta X_{gi}, \Delta P_{ri}, \Delta P_{gi}, \Delta P_{evi}, \int \Delta ACE_i\}$, while $u_i(t) = \Delta P_{ci}$ represents input, and $d_i(t) = \{\Delta P_{di}, \Delta P_{tiei}\}$ represents disturbance vector. Further, the expression for frequency deviation (Δf_i) and area control error (ACE_i) of ith area are given as

$$\Delta f_i = \frac{1}{sM_i + D_i}(\Delta P_{gi} + \Delta P_{evi} - \Delta P_{rfbi} - \Delta P_{di} - \Delta P_{tiei}). \quad (11)$$

$$ACE_i = \beta_i \Delta f_i + \Delta P_{tiei}. \quad (12)$$

$\Delta P_{rfbi} = 0$, if RFB is not placed in power area. State dynamics for ith area of IPS without RFB are expressed as

$$\dot{x}_i = A_{1i}x_i(t) + B_{1i}u_i(t) + W_{1i}d_i(t) \quad (13)$$

Where, A_{1i}, and B_{1i}, and W_{1i} denote the state, input, and the disturbance matrices for the system without RFB. These matrices are derived as below.

$$A_{1i} = \begin{bmatrix} -\frac{D_i}{M_i} & 0 & 0 & \frac{1}{M_i} & \frac{1}{M_i} & 0 \\ -\frac{K_{gi}}{R_i T_{gi}} & -\frac{1}{T_{gi}} & 0 & 0 & 0 & 0 \\ 0 & \frac{K_{ti}}{T_{ti}} & -\frac{1}{T_{ti}} & 0 & 0 & 0 \\ 0 & \frac{K_{ti}K_{ri}}{T_{ti}T_{ri}} & \frac{T_{ti}-K_{ri}}{T_{ti}T_{ri}} & -\frac{1}{T_{ri}} & 0 & 0 \\ 0 & 0 & 0 & 0 & -\frac{1}{T_{evi}} & 0 \\ \beta_i & 0 & 0 & 0 & 0 & 0 \end{bmatrix}$$

$$B_{1i} = \begin{bmatrix} 0 & \frac{\alpha_{gi}K_{gi}}{T_{gi}} & 0 & 0 & \frac{\alpha_{ei}K_{evi}}{T_{evi}} & 0 \end{bmatrix}^T$$

$$W_{1i} = \begin{bmatrix} -\frac{1}{M_i} & 0 & 0 & 0 & 0 & 0 \\ -\frac{1}{M_i} & 0 & 0 & 0 & 0 & 1 \end{bmatrix}^T$$

State vector for system with RFB is $x_i(t) = \{\Delta f_i, \Delta X_{gi}, \Delta P_{ri}, \Delta P_{gi}, \Delta P_{evi}, \Delta P_{rfbi}, \int \Delta ACE_i\}$, and with input and disturbance considered same as in without RFB case, the state dynamics for each area (ith area) of IPS with RFB placed in system are expressed as

$$\dot{x}_i = A_{2i}x_i(t) + B_{2i}u_i(t) + W_{2i}d_i(t) \quad (14)$$

Where, A_{2i}, B_{2i}, and W_{2i} notify state, input, and disturbance matrices, in that order, for ith area, and are derived as given below

$$A_{2i} = \begin{bmatrix} -\frac{D_i}{M_i} & 0 & 0 & \frac{1}{M_i} & \frac{1}{M_i} & -\frac{1}{M_i} & 0 \\ -\frac{K_{gi}}{R_i T_{gi}} & -\frac{1}{T_{gi}} & 0 & 0 & 0 & 0 & 0 \\ 0 & \frac{K_{ti}}{T_{ti}} & -\frac{1}{T_{ti}} & 0 & 0 & 0 & 0 \\ 0 & \frac{K_{ti}K_{ri}}{T_{ti}T_{ri}} & \frac{T_{ti}-K_{ri}}{T_{ti}T_{ri}} & -\frac{1}{T_{ri}} & 0 & 0 & 0 \\ \left(\frac{1}{Trfbi} - \frac{D_i}{M_i}\right)K_{rfbi} & 0 & 0 & \frac{K_{rfbi}}{M_i} & \frac{K_{rfbi}}{M_i} & \left(\frac{K_{rfi}}{Trfb} - \frac{K_{rfbi}}{M_i}\right) & 0 \\ \beta_i & 0 & 0 & 0 & 0 & 0 & \end{bmatrix}$$

$$B_{2i} = \begin{bmatrix} 0 & \frac{\alpha_{gi}K_{gi}}{T_{gi}} & 0 & 0 & \frac{\alpha_{ei}K_{evi}}{T_{evi}} & 0 & 0 \end{bmatrix}^T$$

$$W_{2i} = \begin{bmatrix} -\frac{1}{M_i} & 0 & 0 & 0 & 0 & -\frac{K_{rfbi}}{M_i} & 0 \\ -\frac{1}{M_i} & 0 & 0 & 0 & 0 & -\frac{K_{rfbi}}{M_i} & 1 \end{bmatrix}^T$$

B. Optimal State Feedback Controller

Design of the controller follows with state equation of linear time invariant (LTI) system being available and feedback gain matrix of controller can then be determined through the solution of algebraic Riccati equation. For a given LTI system

$$\dot{x}(t) = Ax(t) + Bu(t). \quad (15)$$

Optimal solution of controller is designed by minimising a suitable objective cost function, which is taken here as

$$J = \int (x'(t)Qx(t) + u'(t)Ru(t))dt \quad (16)$$

$Q \geq 0$ and $R > 0$ Where, Q denotes state cost weighting matrix of n (no. of states) dimensions and is square semi-definite, while R designates control cost weighting matrix of k (no. of inputs) dimensions and is positive definite. Q and R have noticeable impact on performance of regulator/controller, it should, therefore, be chosen carefully. Feedback control input for system is defined as

$$u(t) = -Kx(t). \quad (17)$$

Algebraic Riccati equation is given by

$$A'P + PA - PBR^{-1}B'P + Q = 0. \quad (18)$$

To minimise cost function in Eqn. (16), and to optimise controlled input, algebraic Riccati equation returns a unique solution of P and then state feedback control matrix K is computed as

$$K = R^{-1}B'P. \quad (19)$$

With control law in (17), closed loop system is described as

$$x(t) = (A - BK)x(t). \quad (20)$$

Stability and robustness of this closed loop system can be seen with the Lyapunov function and this LQR methodology guarantees stability, with R and Q satisfying their respective definiteness conditions, and returns static controller gain matrix which results in closed loop system of same order as open loop system [34].

Distributed controller is designed utilising this methodology and framing state model for each area of the system with tie line power considered as an added disturbance vector in individual areas. The gain constant matrix is computed with 'lqr' command in MATLAB. The instant study considers Q and R as identity matrices of appropriate dimension. System of Fig. 1 is simulated with controller and interconnections and the results are analysed. Table III presents the system parameters that are referred from [21] and [35].

4. RESULTS AND DISCUSSION

System is simulated in MATLAB 2021-a version and controller is designed in .m file and performance is assessed in terms of frequency regulation for various operating

TABLE III. System Parameters

Component	Parameters	Area-1,2,3,4
Power system	Power system inertia	M_i 0.1667
	Power system damping coefficient	D_i 0.0083
Reheated thermal Turbine	Turbine time constant	T_{ti} 0.3
	Turbine gain constant	K_{ti} 1
	Governor time constant	T_{gi} 0.08
	Governor gain constant	K_{gi} 1
	Bias Constant	β_1 .425
	Droop characteristics	R_i 2.4
	Thermal turbine participation factor	α_{gi} 0.9
	Reheated thermal unit time constant	T_{ri} 10
	Reheated thermal unit gain constant	K_{ri} 0.5
Electrical Vehicle	EV time constant	T_{evi} 1
	EV gain constant	K_{evi} 1
	EV participation factor	α_{ei} 0.1
Redox Flow Battery	RFB reset time constant	T_{rfi} 0.78
	RFB reset gain constant	K_{rfi} 1
	RFB gain constant	K_{rfbi} 1.8
HVDC Link	Time constant	K_{dci} 1
	Gain constant	T_{dci} 1
AC Link	Synchronising coefficient	$2\pi T_{12}$ 0.1633
TCPS Link	Time constant	T_{tcpsi} 0.1
	Gain constant	K_{tcpsi} 1

conditions under the following four scenarios.
Scenario-I Impact study of interconnections and RFB under open loop (without controller).
Scenario-II Impact study of RFB under closed loop (with controllers) and relative performance assessment.
Scenario-III Performance evaluation under varying state and cost weighting matrices.
Scenario-IV Performance evaluation under uncertainties (renewable disturbances and time delay).

A. *Scenario-I Impact Study of Interconnections and RFB Under Open Loop (Without Controller)*

In this scenario, system is investigated, under open loop (without controller) and subjected to 1% step load change, on two accounts: i) with different configurations of interconnections i.e. positioning of HVDC link, and TCPS link in series with AC Link and ii) incorporating RFB and other ESDs in all four areas, and the response is compared and contrasted. Figures 3 and 4 showcase frequency and tie-line power dynamics of whose analysis reveals that with AC link alone, the response is the most oscillatory, while placement of TCPS in series with AC link improves the response further, which gets even better with both TCPS and HVDC along with AC link in the sense that the nature of response becomes less and less oscillatory. Further, the incorporation of various ESDs (RFB, SMES, UC, FESS, and conventional BESS) in the system along with interconnections of all links improves the response way more. Relative analysis of the improvement brought about by the ESDs shows that the response with either of the two: RFB and SMES, compared to UC, FESS, and conventional BESS, is the best and gets smoothened by almost 90% with the highest peak of frequency response remaining under 0.0065 whereas, in case of tie line power, the oscillations are damped out completely. Placement of RFB in each area supports power system in the event of sudden loading and helps regulate the frequency effectively.

B. *Scenario-II Impact Study of RFB Under Closed Loop (With Controllers) and Relative Performance Assessment*

In this scenario, investigations are conducted two fold: i) relative impact study of RFB vis-à-vis other ESDs, and ii) study of efficacy of proposed distributed optimal controller vis-à-vis PI and PID controllers. For both parts, 0.01 p.u. change of load in area-1 serves as the disturbance. Now, as a first part, simulations are conducted without and with various ESDs (considering one at a time), with LQR based distributed optimal controller in place. In the second part, the system is simulated with the proposed LQR based distributed optimal, PI, and PID controllers, one at a time, considering RFB integrated in all four-areas. Figures 5 and 6 showcase the relative performance of different ESDs from which it can be visualised that it is RFB that outperforms all other ESDs in suppressing frequency and tie-line oscillations most quickly, meaning thereby that settling time comes out to be the least. Not only this, the system response with RFB is less oscillatory. Table IV presents the settling times with different ESDs wherein it can be clearly seen that in case of RFB, the value is the least i.e. 7.438 sec. Figure 7 displays frequency and tie-line power dynamics with LQR based distributed optimal, proposed in the instant study, as against PI and

PID controllers bringing out proposed controller as most effective of all three with settling time not only being the least but the gap upto the next nearer value is also very large. Table V puts in place the data of settling time for all the three controllers. When compared with the nearest similar existing work [1], the performance in the instant study is improved in terms of settling time.

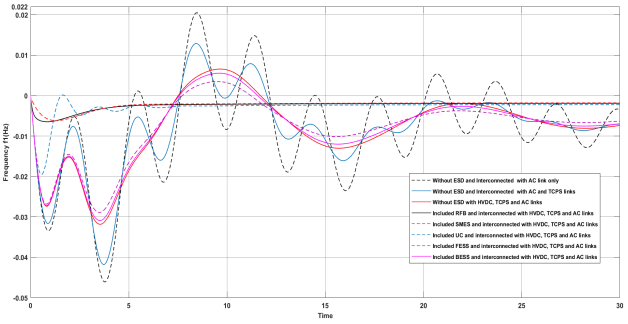

Figure 3. Frequency response without controller

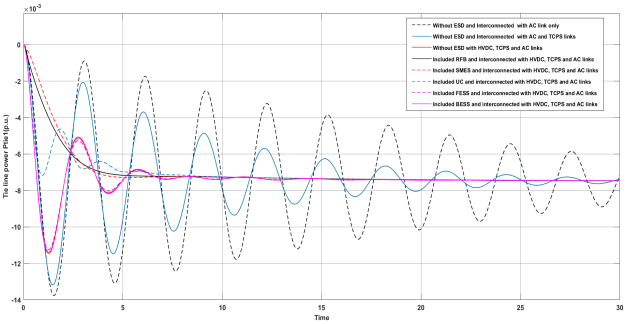

Figure 4. Tie Line Power response without controller

C. *Scenario-III Performance Evaluation Under Varying State and Cost Weighting Matrices*

LQR controller design methodology depends upon choice of state weighting and cost weighting matrices, so in this section, investigation on the controller performance is conducted to assess as to how variations in these two matrices affect the frequency response under 0.1 p.u. step up in load. The frequency response under varying R and Q are shown in Fig. 8 and 9, respectively where from it can be clearly inferred that dynamic performance shows less sensitivity to variations in R as compared to variations in Q. Also, the frequency settles faster for lesser values of R. The important observation is that selection of Q is very critical and more significant relative to R and therefore, it should be chosen wisely. In the instant study, system dynamics go on becoming more and more oscillatory resulting in large peak value of frequency for $Q > I$ and likewise the system frequency deviations are large and not converging towards zero value for $Q < 0.5I$, where I is the identity matrix.

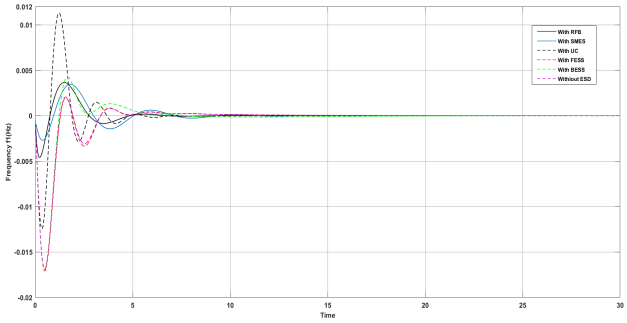

Figure 5. Frequency response with and without ESDs

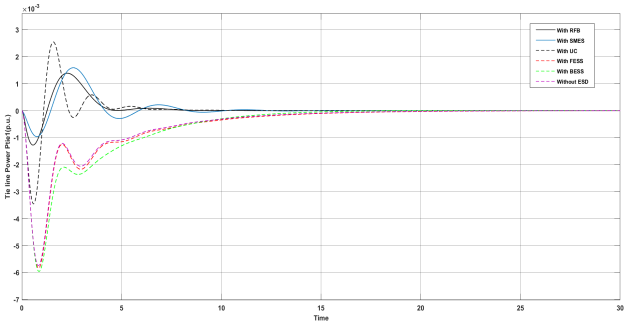

Figure 6. Tie line power response with and without ESDs

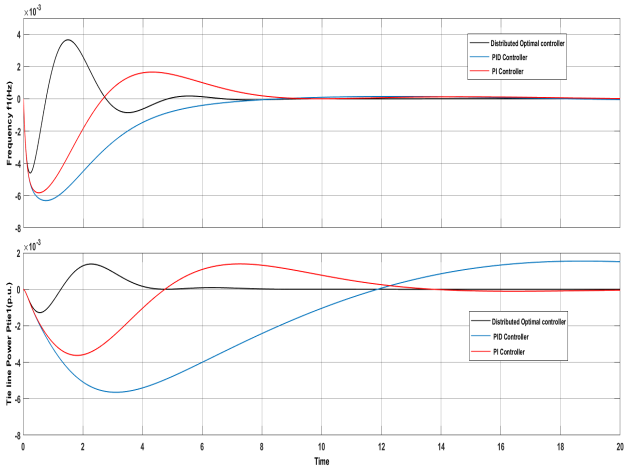

Figure 7. Tie line power response with and without ESDs

D. *Scenario-IV Performance Evaluation Under Uncertainties (Renewable Disturbances and Time Delay)*

Proposed controller is evaluated under uncertain loading conditions, mimicking the intermittency of renewable sources of power, in this case, wind and PV power. These conditions are realized through simulation utilising white noise block in MATLAB and the following formulae for wind and PV powers [36], respectively.

TABLE IV. Settling time with different ESDs

Type of ESD	RFB	SMES	UC	FESS	Conventional BESS
Settling time (s)	7.438	9.124	8.235	13.514	18.123

TABLE V. Settling time with different controllers

Type of controller	Proposed	PI	PID
Settling time (s)	7.438	31.318	30.377

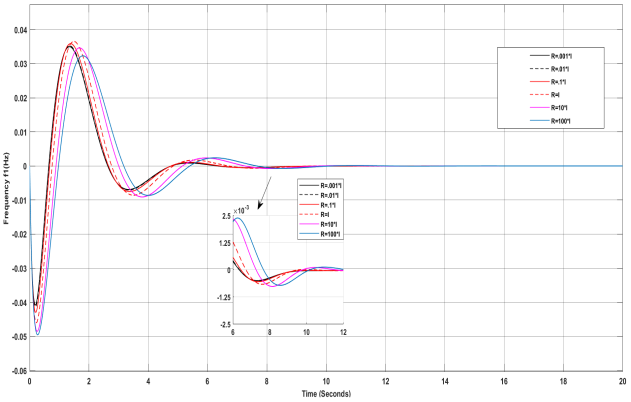

Figure 8. Frequency response under varying R

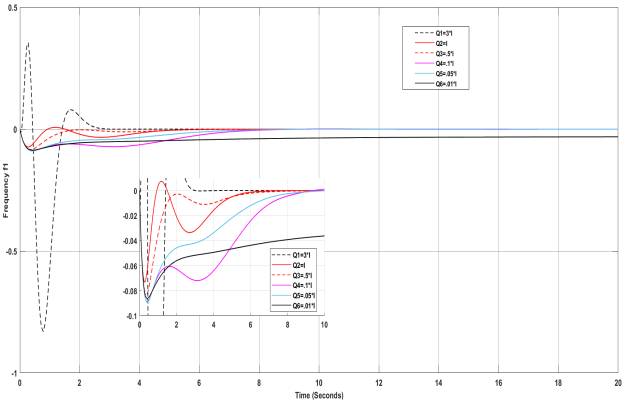

Figure 9. Frequency response under varying Q

Wind power extraction from wind turbine is governed by the following expression

$$P_w = \frac{1}{2}\rho A C_p(\lambda,\beta)V_W^3 \tag{21}$$

Where, ρ denotes air density and A the swept area of wind turbine blade, while power coefficient of wind turbine is given by

$$C_p(\lambda,\beta) = C_1\left(\frac{C_1}{\lambda_i} - C_3\beta - C_4\beta_2 - C_5\right)e^{-\frac{C_6}{\lambda_i}} + C_7\lambda_T \tag{22}$$

Where, β, λ_T, and λ_i stand for pitch angle, optimum tip speed ratio (TSR), and interrupted TSR of rotor blade of WT, respectively, and λ_T and λ_i are computed as follows

$$\lambda_T = \frac{wR}{V}. \tag{23}$$

$$\frac{1}{\lambda_i} = \frac{1}{\lambda_T + 0.08\beta} - \frac{0.035}{1+\beta^3}. \tag{24}$$

Wind turbine operates at an optimum TSR for varying wind speed and w, V, and R stand for rotor speed, wind speed and radius of rotor blade, respectively. Solar power variation from PV generator is given by

$$\Delta P_{solar} = 0.6\sqrt{P_{solar}} \tag{25}$$

PV generated power variance and wind speed are not consistent and it can be modelled utilising white noise block as referred in [36].
PW = 3 MW, V = 12 m/s, ρ = 1.225 kgm^2, A = 5905 m^2, R = 43.36 m, n = 22.5 rpm, C_1 = 0.3915, C_2 = 116, C_3 = 0.4, C_4 = 0, C_5 = 5, C_6 = 21, C_7 = 0.0192

The variable load incorporating these uncertainties is shown in Fig. 10, in which the load is 0.1 p.u step until 50 sec, then after wind uncertainty is added that brings in randomness in the load and the combined load gets stepped up around 0.2 p.u. onwards 50 sec until 100 sec, and then gets added up the uncertain load of PV bringing the total load to around 0.31 p.u. and this total load stays for the remaining period. Figure 11 showcases corresponding frequency and tie-line power dynamics, showing oscillations against these changeovers of loads settling quickly with the proposed controller, which establishes the efficacy of the controller even under uncertain loads, while without controller, there remain offsets all along with frequency and tie-line power excursions never dying down and converging to nominal values.

To establish the robustness of the proposed controller even further, system non-linearity in the form of time delay is considered and Fig. 12 shows the frequency dynamics of area-1 under 0.1 p.u. step-up of load corresponding to fixed time delays of 0.12 s, 0.14 s, and 0.16 s. The system response (Fig. 12) is smooth, almost non-oscillatory, and settles soon which goes on to prove the proposed controller as robust against these delays. Recent similar research works have neither considered the time delay non linearity nor the solar and wind power uncertainties [1] [25][30].

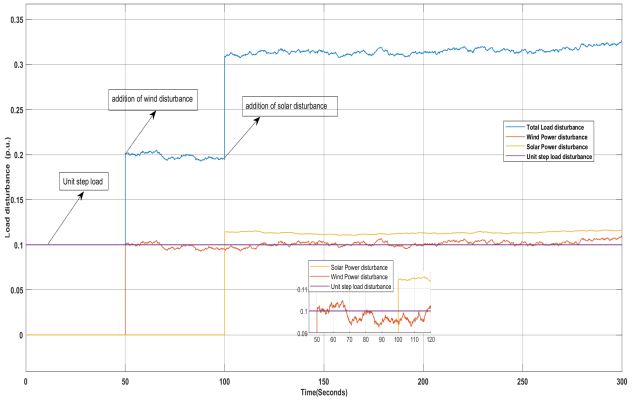

Figure 10. Varying load disturbance considering renewable energy disturbances

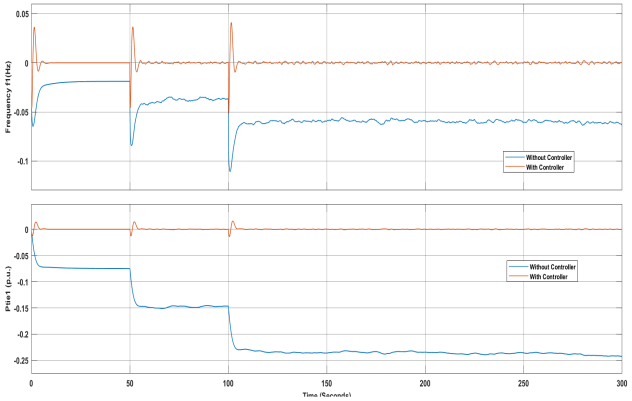

Figure 11. Frequency and tie line power response under renewable energy disturbances

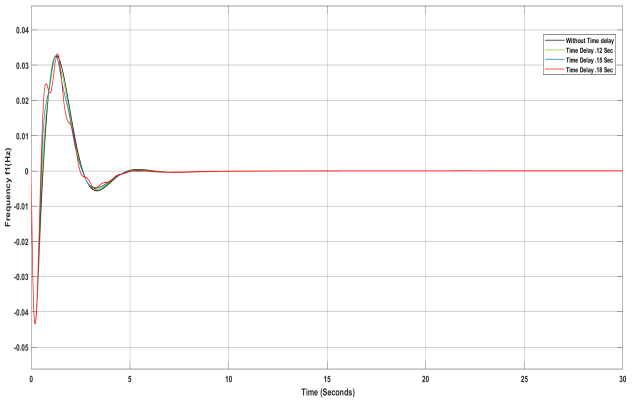

Figure 12. Frequency response under varying time delays

5. CONCLUSION

It is established here that with RFB, controller performance is enhanced the most and the response is more robust and faster to stabilise frequency oscillations on occurrence of sudden load perturbation. Distributed LQR optimal controller is the control strategy used for the large power system, considering interconnections of HVDC, AC link, and TCPS besides the ESDs. The relative assessment of the improvement in system dynamics brought about by various interconnections of HVDC, AC link, and TCPS and combinations thereof is also demonstrated and analysed. The system performance with multiple links gets better in comparison to the case when AC link alone is connected. This controller is found highly robust against renewable uncertainties and time delay non linearity as well. The proposed distributed controller, designed using presented methodology, is much easier and can be utilised in future along with advanced methodologies. The study can be extended in future by incorporating modified controllers to improve system performance, power areas may include more renewable energy sources and non-linearities thereof, and also more than one EVs can be considered connected in the system with their random arrival and exit.

ABBREVIATIONS

IPS	Interconnected Power System
ESD	Energy Storage
HVDC	High Voltage Direct Current
LQR	Linear Quadratic Regulator
RFB	Redox Flow Battery
LFC	Load Frequency Control
TCPS	Thyristor Controlled Phase Shifter
UC	Ultra-capacitor
FESS	Fly wheel Energy Storage System
EV	Electrical Vehicles
SMES	Superconducting Magnetic Energy Storage
BESS	Battery Energy Storage System

REFERENCES

[1] C. N. S. Kalyan, B. S. Goud, C. R. Reddy, M. Bajaj, N. K. Sharma, H. H. Alhelou, P. Siano, and S. Kamel, "Comparative performance assessment of different energy storage devices in combined lfc and avr analysis of multi-area power system," *Energies*, vol. 15, no. 2, 2022.

[2] J. Morsali, K. Zare, and M. Tarafdar Hagh, "Performance comparison of tcsc with tcps and sssc controllers in agc of realistic interconnected multi-source power system," *Ain Shams Engineering Journal*, vol. 7, no. 1, pp. 143–158, 2016.

[3] N. Pathak, A. Verma, T. S. Bhatti, and I. Nasiruddin, "Modeling of hvdc tie links and their utilization in agc/lfc operations of multi-area power systems," *IEEE Transactions on Industrial Electronics*, vol. 66, no. 3, pp. 2185–2197, 2019.

[4] M. Langwasser, G. D. Carne, M. Liserre, and M. Biskoping, "Enhanced grid frequency support by means of hvdc-based load control," *Electric Power Systems Research*, vol. 189, p. 106552, 2020.

[5] G. Sharma, "Performance enhancement of a hydro-hydro power system using rfb and tcps," *International Journal of Sustainable Energy*, vol. 38, no. 7, pp. 615–629, 2019.

[6] P. Bhatt, S. Ghoshal, and R. Roy, "Coordinated control of tcps and smes for frequency regulation of interconnected restructured power systems with dynamic participation from dfig based wind farm," *Renewable Energy*, vol. 40, no. 1, pp. 40–50, 2012.

[7] L. S. Kumar, D. Ananth, Y. V. P. Kumar, D. J. Pradeep, C. P. Reddy, and E. Ariwa, "Use of super conductor magnetic energy storage system and facts devices for two-area load frequency control having synchronous generators and dfig wind generators," *International Journal of Computing and Digital Systems*, vol. 10, no. 1, pp. 1227–1238, 2021.

[8] A. Kumar and S. Shuhag, "Impact of tcps, smes and dfig on load frequency control of nonlinear power system using differential evolution algorithm," *J. Inst. Eng. India Ser. B*, vol. 100, pp. 153–167, 2019.

[9] O. Krishan and S. Suhag, "An updated review of energy storage systems: Classification and applications in distributed generation power systems incorporating renewable energy resources," *International Journal of Energy Research*, vol. 43, no. 12, pp. 6171–6210, 2019.

[10] S. Koohi-Fayegh and M. A. Rosen, "A review of energy storage types, applications and recent developments," *Journal of Energy Storage*, vol. 27, p. 101047, 2020.

[11] "Handbook on battery energy storage system," 2018.

[12] P. Alotto, M. Guarnieri, and F. Moro, "Redox flow batteries for the storage of renewable energy: A review," *Renewable and sustainable energy reviews*, vol. 29, pp. 325–335, 2014.

[13] I. Chidambaram and B. Paramasivam, "Control performance standards based load-frequency controller considering redox flow batteries coordinate with interline power flow controller," *Journal of power sources*, vol. 219, pp. 292–304, 2012.

[14] D. H. Tungadio and Y. Sun, "Load frequency controllers considering renewable energy integration in power system," *Energy Reports*, vol. 5, pp. 436–453, 2019.

[15] I. A. Khan, H. Mokhlis, N. N. Mansor, H. A. Illias, L. Jamilatul Awalin, and L. Wang, "New trends and future directions in load frequency control and flexible power system: A comprehensive review," *Alexandria Engineering Journal*, vol. 71, pp. 263–308, 2023.

[16] S. K. Pandey, S. R. Mohanty, and N. Kishor, "A literature survey on load–frequency control for conventional and distribution generation power systems," *Renewable and Sustainable Energy Reviews*, vol. 25, pp. 318–334, 2013.

[17] A. Fathy and A. G. Alharbi, "Recent approach based movable damped wave algorithm for designing fractional-order pid load frequency control installed in multi-interconnected plants with renewable energy," *IEEE Access*, vol. 9, pp. 71 072–71 089, 2021.

[18] K. S. Ko and D. K. Sung, "The effect of ev aggregators with time-varying delays on the stability of a load frequency control system," *IEEE Transactions on Power Systems*, vol. 33, no. 1, pp. 669–680, 2018.

[19] A. Kumar and Sathans, "Hybrid bacterial foraging enhanced pso algorithm for load frequency control of hydro-thermal multi-area power system and comparative analysis," *International Journal of Computing and Digital Systems*, vol. 9, no. 1, pp. 129–38, 2020.

[20] S. H. Shahalami and D. Farsi, "Analysis of load frequency control in a restructured multi-area power system with the kalman filter and the lqr controller," *AEU - International Journal of Electronics and Communications*, vol. 86, pp. 25–46, 2018.

[21] T. N. Pham, H. Trinh, and L. V. Hien, "Load frequency control of power systems with electric vehicles and diverse transmission links using distributed functional observers," *IEEE Transactions on Smart Grid*, vol. 7, no. 1, pp. 238–252, 2016.

[22] H. Haes Alhelou, M. E. Hamedani Golshan, and N. D. Hatziargyriou, "Deterministic dynamic state estimation-based optimal lfc for interconnected power systems using unknown input observer," *IEEE Transactions on Smart Grid*, vol. 11, no. 2, pp. 1582–1592, 2020.

[23] A. Singh and Sathans, "Minimum order quasi-decentralized functional observer (moqdfo) for frequency regulation in multi-area power system with dc link and tcps," *International Journal of Computing and Digital Systems*, vol. 11, no. 1, pp. 713–724, 2022.

[24] E. Vlahakis, L. Dritsas, and G. Halikias, "Distributed lqr design for a class of large-scale multi-area power systems," *Energies*, vol. 12, no. 14, p. 2664, 2019.

[25] A. M. A. Soliman, M. Bahaa Eldin, and M. Ahmed Mehanna, "Application of woa tuned type-2 flc for lfc of two area power system with rfb and solar park considering tcps in interline," *IEEE Access*, vol. 10, pp. 112 007–112 018, 2022.

[26] M. Sharma, S. Dhundhara, and R. S. Sran, "Impact of hybrid electrical energy storage system on realistic deregulated power system having large-scale renewable generation," *Sustainable Energy Technologies and Assessments*, vol. 56, p. 103025, 2023.

[27] M. Joshi, G. Sharma, and E. Çelik, "Load frequency control of hydro-hydro power system using fuzzy-pso-pid with application of uc and rfb," *Electric Power Components and Systems*, vol. 51, no. 12, pp. 1156–1170, 2023.

[28] C. N. S. Kalyan, B. S. Goud, C. R. Reddy, M. Bajaj, and G. S. Rao, "Smes and tcsc coordinated strategy for multi-area multi-source system with water cycle algorithm based 3dof-pid controller," *Smart Science*, vol. 11, no. 1, pp. 1–15, 2023.

[29] S. K. Ramoji, L. Chandra Saikia, B. Dekaraja, M. K. Behera, and S. Kumar Bhagat, "Repercussions of smes and hvdc link in amalgamated voltage and frequency regulation of multi-area multi-unit interconnected power system," pp. 1–6, 2022.

[30] M. Bhuyan, D. C. Das, A. K. Barik, and S. C. Sahoo, "Performance assessment of novel solar thermal-based dual hybrid microgrid system using cboa optimized cascaded pi-tid controller," *IETE Journal of Research*, pp. 1–18, 2022.

[31] S. Rangi, S. Jain, and Y. Arya, "Utilization of energy storage devices with optimal controller for multi-area hydro-hydro power system under deregulated environment," *Sustainable Energy Technologies and Assessments*, vol. 52, p. 102191, 2022.

[32] K. Enomoto, T. Sasaki, T. Shigematsu, and H. Deguchi, "Evaluation study about redox flow battery response and its modeling," *IEEJ Trans. PE*, vol. 122, pp. 554–560, 04 2002.

[33] A. Prakash and S. Parida, "Combined frequency and voltage stabilization of thermal-thermal system with upfc and rfb," in *2020*

IEEE 9th Power India International Conference (PIICON). IEEE, pp. 1-6, 2020.

[34] R. D. Joslin and D. N. Miller, "Fundamentals and applications of modern flow control," 2009.

[35] N. R. Babu, L. C. Saikia, S. K. Bhagat, S. K. Ramoji, D. Raja, and M. K. Behera, "Impact of wind system and redox flow batteries on lfc studies under deregulated scenario," in *2020 3rd International Conference on Energy, Power and Environment: Towards Clean Energy Technologies*, pp. 1-6, 2021.

[36] G. Magdy, H. Ali, and D. Xu, "Effective control of smart hybrid power systems: Cooperation of robust lfc and virtual inertia control systems," *CSEE Journal of Power and Energy Systems*, vol. 8, no. 6, pp. 1583–1593, 2022.

Archana Singh is pursuing her PhD in the area of power quality and voltage control in smart grids from the School of Renewable Energy and Efficiency, National Institute of Technology, Kurukshetra, Haryana, India. Her research interests include control of hybrid energy systems, estimated distributed control of large power system.

Sathans Suhag received his PhD degree in the area of intelligent control and its applications to power systems from the National Institute of Technology Kurukshetra, Haryana, India, in 2012 where, he is currently serving as Professor. His research interests include intelligent control techniques, control issues in hybrid energy systems, evolutionary algorithms and their applications in power systems.